Japanese Journal of Applied Physics **51** (2012) 074004 **REGULAR PAPER**
**DOI:** 10.1143/JJAP.51.074004

# Asymmetrically Doped GaAs/AlGaAs Double-Quantum-Well Structure for Voltage-Tunable Infrared Detection

Jae Kyu Choi[1], Nizami Vagidov[1]*, Andrei Sergeev[1], Stefan Kalchmair[2], Gottfried Strasser[1,2], Fedir Vasko[1], and Vladimir Mitin[1]

[1]*Department of Electrical Engineering, University at Buffalo, SUNY, Buffalo, NY 14260-1920, U.S.A.*
[2]*Center for Micro- and Nanostructures, TU Vienna, Vienna 1040, Austria*

Received March 29, 2012; accepted May 17, 2012; published online June 29, 2012

We fabricate, characterize, and analyze tunable mid-infrared photodetectors based on asymmetrically doped coupled quantum well GaAs/AlGaAs structures. The peak of photoresponse detection varies from 7.5 to 11.1 μm when switching bias from −5 to +5 V. The spectral tunability is defined by the interplay of several effects. First, the electron energy levels are shifted due to the Stark effect. Second, the applied electric field causes the charge redistribution in the coupled wells and shift of electron energy levels due to modification of self-consistent potential. Here we show that effect of electric field on tunneling processes (the Poole–Frenkel effect) and the field-induced decrease of thermo-emission barrier (the Fowler–Nordheim effect) also play a critical role in photoelectron kinetics, strongly enhancing the carrier extraction from quantum wells. The model which takes into account Poole–Frenkel and Fowler–Nordheim effects provides a quantitative description of the data obtained.


## 1. Introduction

Quantum well IR photodetectors (QWIP) have attracted considerable attention due to a variety of applications such as remote sensing, thermal imaging, industrial and environmental monitoring.[1–3] The well-established growth and processing techniques of the $A_3B_5$-based heterostructures open a wide range of possibilities for bandgap engineering and intersubband transitions for detection of IR radiation.[4–6] QWIPs are promising candidates for multi-color sensing in the spectral range from THz to mid-IR. Voltage-switchable and voltage-tunable QWIPs have been studied in a number of works. Various approaches for the design of voltage-tunable and voltage-switchable QWIPs have been proposed. One of the possible designs is based on two stacks of QWIP structures with three electrical terminals, which allows one to bias each QWIP independently and detect two wavelengths simultaneously.[7–9] Another design includes several stacked QWIP structures separated by thin heavily doped layer with two electrical terminals.[10] Within this approach, the detection wavelength can be switched by changing the applied voltage. In all such devices, the voltage-induced shift of electron levels and modification of the corresponding IR transitions is realized via several mechanisms, such as quantum-confined Stark effect,[11] graded barriers,[12] and asymmetric step wells,[13] or charge redistribution.[14,15] Charge sensitive QWIPs based on double-quantum-well (DQW) transistor have been recently demonstrated.[16–18] More effective voltage tunability and switching can be expected in asymmetrically doped DQWs due to superposition of external field with doping-induced built-in electric field.

In this paper, we show that asymmetrical doping of DQW-structure provides two-color sensing as well as voltage-switchable and voltage-tunable photoresponse. The DQW structure is formed by 25 identical stages [the potential profiles of left-most and right-most DQWs are slightly different due to contacts, see Fig. 1(a)]. The DQWs have been designed to support solely two intersubband transitions from ground states to the excited states. Therefore, the photoresponse to IR radiation has two spectral components. Both components are strongly affected by the bias voltage $V_b$. The voltage tunability of the photoresponse spectrum is mainly defined by three mechanisms. First, the electron energy levels are shifted due to the Stark effect. Second, the applied electric field causes a charge redistribution in the coupled wells and shift of electron energy levels due to modification of self-consistent potential. Third, the electric field enhances tunneling and thermo-activation processes due to a reduction of the width and height of the triangular barriers which separate extended states from excited states [see Fig. 1(a)]. Here we limit our consideration by relatively low fields that do not generate electric field domains[19] and other instabilities.

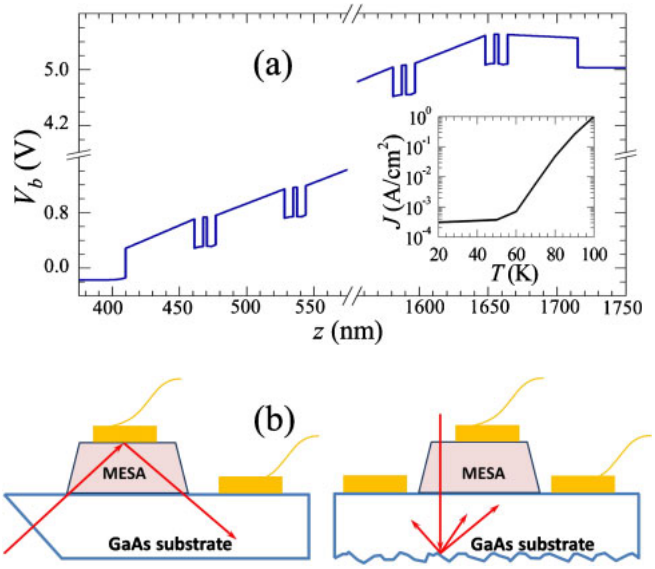


**Fig. 1.** (Color online) (a) Energy band diagram of 25 period DQW structure under bias $V_b = +5$ V. (b) Schematic view of photoexcitation geometry through substrate with 45° facet (left) or under diffuse reflection of normally incident radiation (right). Inset shows dark current density, $J$, versus temperature, $T$, at bias $V_b = +3$ V.

To provide effective coupling of IR radiation to our QWIP devices, we compare the following two schemes. In the first scheme, the radiation is incident on the 45°-angle facet of substrate and in the second scheme the coupling to normal incident radiation is enhanced by the diffuse reflector [see Fig. 1(b)].[20] Without diffuse reflector, the coupling to normally incident IR radiation, associated with a violation

*E-mail address: nizami@buffalo.edu

of the polarization selection rule for intersubband transitions, is small.[21)]

We studied the voltage-tunable photocurrent in our asymmetric structures in the temperature interval from 20 to 100 K, which upper value is limited by the noise current. As it is shown in the inset of Fig. 1(a), the dark current and corresponding noise current increase exponentially with temperature. The photoresponse slowly decreases with temperature and at $T > 100$ K the photocurrent becomes smaller than the noise current.

The paper is organized as follows. In §2 we describe the design and fabrication of our QWIP structures. The results of measurements are presented and discussed in §3. In §4 we analyze the obtained experimental data and compare them with the results of modeling.

## 2. QWIP Design and Fabrication

To calculate the photo-induced transitions we performed self-consistent calculations, which take into account charge redistribution in asymmetrically doped DQWs. For our calculations we used the nextnano$^3$ software[22)] which is a flexible and effective tool for the analysis of photodetectors.[23–27)] Our modeling shows that tunability is improved in structures where the excited states are located close to the extended states. The schematic epitaxial layer structure of a device with high tunability is shown in Fig. 2. It is based on the coupled quantum wells composed of a 6.5 nm GaAs layer Si-$\delta$-doped with sheet concentration $5 \times 10^{11}$ cm$^{-2}$ and a 6.5 nm undoped GaAs layer separated by a 3.1-nm-thick $Al_{0.2}Ga_{0.8}As$ layer. The device consists of 25 DQW stages separated by 50 nm $Al_{0.2}Ga_{0.8}As$ barriers (see Fig. 2). We present in Fig. 3 the conduction band diagram of a single stage, which consists of two coupled QWs. In this figure we also demonstrate modification of wave functions and the energy levels due to the bias voltage ($V_b = -5$, 0, and +5 V). The calculated populations of the first two tunnel-coupled levels at $T = 70$ K as a function of the voltage are as follows: 99 and 1%, 95 and 5%, and 76 and 24%, at −5, 0, and +5 V, respectively. One can see that there is almost no redistribution of electrons between levels for negative $V_b$ while for positive $V_b$, when tunnel coupling increases, a significant redistribution of electrons takes place. Strong coupling of levels near the top of quantum wells is realized for $V_b \neq 0$ since these states are connected to the continuum. Since only the right quantum well is doped, the DQW's band diagram is asymmetric at $V_b = 0$ due to the built-in electric field contribution. The modeling shows larger peak-shift under negative bias which is more symmetric since the built-in electric field compensates the applied bias. In principle, there are four possible transitions between two deep and two shallow levels in a single detection unit. A two-color photoresponse is found because only the lowest level is populated under negative bias [see Fig. 3(a)]. Under positive bias the transitions from the lowest excited state to the extended states via tunneling processes are suppressed and thermoexcitation processes are limited by relatively high barrier [Fig. 3(c)]. Therefore, the lowest excited state weakly contributes to the photocurrent. Using this mechanism the two-color operation is realized in asymmetrically doped DQW structure.

The DQW QWIP structure was grown by molecular beam epitaxy on a semi-insulating GaAs wafer to permit backside

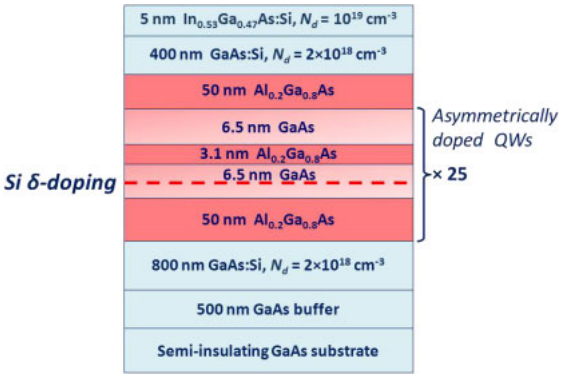


**Fig. 2.** (Color online) Schematic epitaxial layer structure of QWIP with asymmetrically doped detection units.

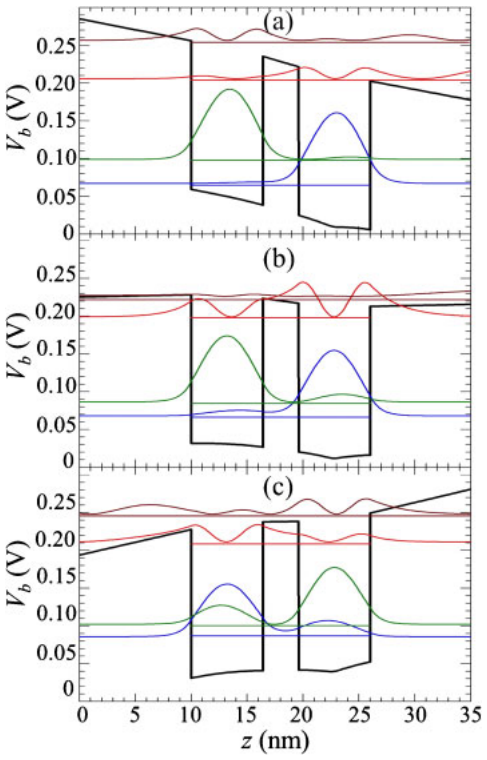


**Fig. 3.** (Color online) Self-consistently calculated potentials and wave functions of the ground and excited states in DQWs at $T = 70$ K under $V_b = -5$ (a), 0 (b), and +5 V (c). The relative populations of the first two tunnel-coupled levels are: 99 and 1% (a), 95 and 5% (b), and 76 and 24% (c), respectively.

illumination (Fig. 2). The growth sequence started with a 500 nm undoped GaAs buffer layer, and was followed by a 800 nm heavily doped ($N_d = 2 \times 10^{18}$ cm$^{-3}$) GaAs contact layer, 25 stages of the detection unit, 400 nm layer of GaAs doped to $2 \times 10^{18}$ cm$^{-3}$ as a contact layer, and finally 5 nm InGaAs layer doped to $10^{19}$ cm$^{-3}$. One unit of the QWIP is composed of 6.5 nm GaAs layer $\delta$-doped with Si with sheet density $5 \times 10^{11}$ cm$^{-2}$ and 6.5 nm undoped GaAs separated by 3.1-nm-thick $Al_{0.2}Ga_{0.8}As$. Each unit is separated by 50 nm $Al_{0.2}Ga_{0.8}As$ barriers. Layer thicknesses and Al concentration are confirmed by an X-ray diffraction measurement after growth. The sample was fabricated into a square mesa structure of $100 \times 100$ μm$^2$ using standard UV lithography, wet chemical etching and metallization techniques. The mesa structures were etched with sulfuric

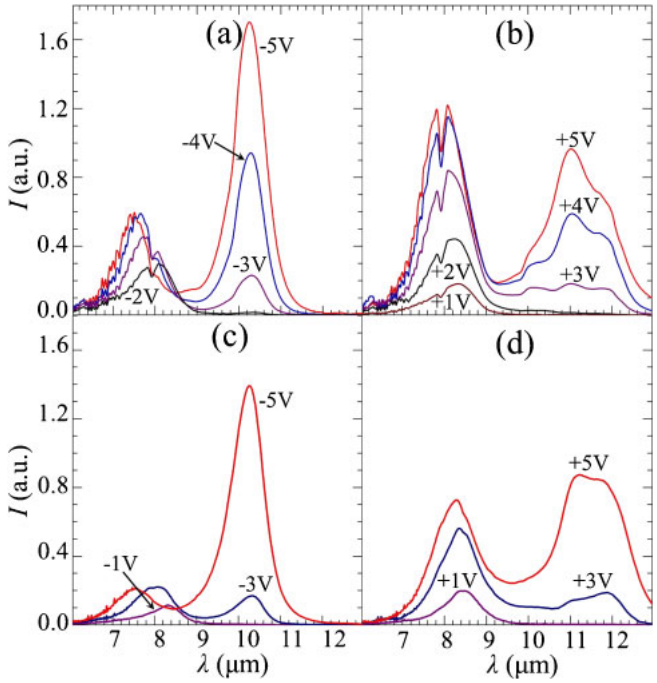


**Fig. 4.** (Color online) Spectral dependencies of photocurrent at $T = 20\,\mathrm{K}$ under negative (a, c) and positive (b, d) bias voltages for the cases of photoexcitation under diffuse reflection of normally incident radiation (a, b) or through 45° facet (c, d).

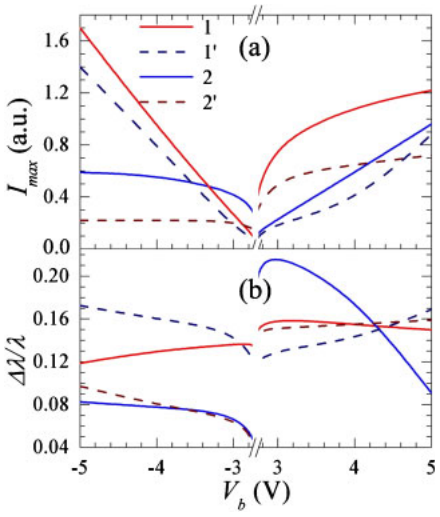


**Fig. 5.** (Color online) (a) Amplitudes of low- and high-energy peaks of photocurrent (marked as 1 and 2, respectively) versus $V_b$ at $T = 20\,\mathrm{K}$. (b) Widths of these peaks versus $V_b$. Solid (1 and 2) and dashed (1′ and 2′) curves correspond to the cases of photoexcitation under diffuse reflection of normally incident radiation or through 45° facet, respectively.

acid ($H_2SO_4 : H_2O_2 : H_2O = 3 : 10 : 450$) at an etch rate of 1.5 nm/s. Ohmic contacts, Ni/Ge/Au/Ni/Au layers with thicknesses of 2/14/28/40/100 nm, respectively, were deposited by e-beam evaporation, followed by rapid thermal annealing for 40 s at 430 °C.

## 3. QWIP Characterization

The spectral density of photocurrent reported in this paper was measured using a Bruker Vertex 70 FTIR spectrometer. The device was mounted inside the continuous-flow He cryostat with a ZnSe window. To enhance optical absorption by the DQWs we illuminated from the backside through a 45° angled facet or used a diffuse reflector. To fabricate 45° angle facet for QWIP structure we used standard polishing techniques. The diffuse reflector was obtained by polishing the backside of the substrate with 3 μm grit polishing pad.[28] These two methods provide effective coupling of IR radiation to our devices, so the photocurrent $I$ can be distinguished from the fluctuating dark current background in the temperature range below 100 K if the bias voltage exceeds 1 V.

The spectral changes of the photocurrent were reliably measured for both bias polarities at temperatures below 70 K (see Fig. 4). As it was discussed in §2 the spectral characteristics of the photoresponse strongly depend on the polarity of the bias voltage due to asymmetric doping. Below 70 K we observe two distinctive peaks. At negative bias [Figs. 4(a) and 4(c)], these two peaks are centered near 7.9 and 10.3 μm wavelengths. These peaks can be attributed to the transitions from the lowest ground state to the excited states, that are effectively coupled to the extended states. For an intermediate bias ($V_b \sim -3\,\mathrm{V}$) both spectral peaks are observed with small overlap. The intensities and widths of the peaks depend on bias voltage. The peak around 10.3 μm, observed only at large magnitude of bias voltages [$V_b < -2.6\,\mathrm{V}$, see Figs. 4(a) and 4(c)], is caused by the supression of the tunneling processes. At low bias voltages [see the band diagram in Fig. 3(b)], the photocurrent is blocked by the 50 nm $Al_{0.2}Ga_{0.8}As$ barriers. However, when increasing the positive bias, the tunneling barrier is lowered down and carriers can escape the quantum wells increasing the photocurrent. The main spectral peaks (7.5 and 10.3 μm under negative bias) shift to 8.3 and 11.1 μm under positive bias. For the same reason as the peak at 10.3 μm is only visible at high negative bias voltage, the photocurrent peak around 11 μm appears only at a large magnitude of the applied positive bias ($V_b \geq 3\,\mathrm{V}$) [see Figs. 4(a) and 4(d)]. Since the upper levels transform into extended states for positive bias, the widths of peaks increase.

## 4. Discussion and Conclusions

Both schemes of coupling of IR radiation to our devices (Fig. 1) yield very similar shapes of the photoresponse [Figs. 4(a)–4(d)]. The amplitudes of high- and low-energy peaks of photocurrent differ up to 2 times under negative bias and about 30% under positive bias [see Fig. 5(a)]. The bias voltage dependences are different for $V_b > 0$ and $V_b < 0$ because of the doping asymmetry. For the same reason, the widths of peaks are also different, as it is shown in Fig. 5(b) where the relative widths $\Delta\lambda/\lambda$ are plotted versus $V_b$. For negative bias the high-energy peaks show narrower linewidth $\Delta\lambda/\lambda \simeq 0.07 - 0.1$ due to transitions between localized states. The linewidths are about $\Delta\lambda/\lambda \simeq 0.15$ for the low-energy peak and for both peaks at positive bias. In addition, $\Delta\lambda/\lambda$ increases up to ~0.2 at $V_b \sim 3\,\mathrm{V}$ when the photoresponse is suppressed.

Spectral and bias dependences of photocurrent are summarized by the contour plots shown in Figs. 6(a) and 6(b) for the both cases of photoexcitation. The largest peak shifts occur at $V_b < 0$ because the doping-induced internal electric field is added to bias voltage and the quantum-confined Stark effect is more pronounced. Also the short-wavelength peaks have larger peak-shift than the long-

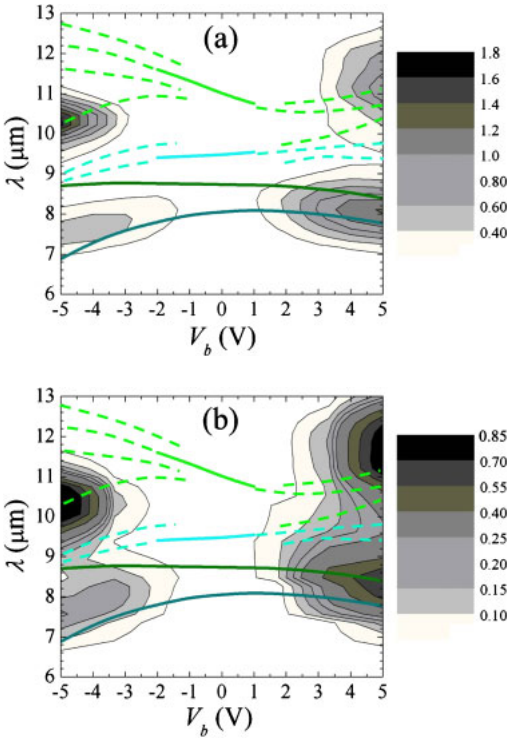


**Fig. 6.** (Color online) Contour plot of photocurrent versus $V_b$ and wavelength, $\lambda$, for the cases of photoexcitation under diffuse reflection of normally incident radiation (a) or through 45° facet (b). Solid and dashed curves correspond to transitions between localized states and from localized to extended states, respectively.

wavelength ones because the transitions into extended states are more sensitive to applied voltage $V_b$. The behavior of photocurrent versus $V_b$ and $\lambda$ is similar to the corresponding transition energies calculated with our self-consistent simulation. In Fig. 6 we plot both the transitions between localized states (solid curves) and transitions to extended states (dashed curves). Note, that these curves give the absorption peak positions while the photocurrent peaks are determined not only by absorption processes but also by thermal generation and capture processes. Due to this, the difference between the calculated transitions and the photocurrent peaks takes place.

Finally we discuss the temperature dependence of the photoresponse. At temperatures below 80 K the photocurrent weakly depends on temperature (a few percent variations). This weak temperature dependence of the photocurrent may be associated by interplay of two opposite effects. The photoemission processes are enhanced with temperature, while photoelectron lifetime decreases with temperature increase. The dark current increases exponentially with temperature [see inset of Fig. 1(a)] and above 80 K the corresponding noise current becomes comparable with the photocurrent. Therefore, at temperatures higher than 100 K the photoresponse measurements are not possible with the available source and detector.

In conclusion, we have designed, grown, and characterized a two-color QWIP based on intersubband transitions in asymmetrically doped coupled QWs. In these structures the effects of electric field on electron states (Stark effect), tunneling processes (Fowler–Nordheim effect), and thermo-activation processes (Poole–Frenkel effect) are inhanced by the asymmetrical doping. These effects provide an effective voltage tunability of spectral photoresponse. In our devices the spectral peaks switch from ~7.5 to ~11.1 μm by reversing the bias polarity. The spectral characteristics are controlled at the intermediate bias voltages. Further improvements in tunability are expected at higher doping levels. In future, these relatively simple and highly scalable devices may be used in multi-element imaging arrays for multi-spectral sensing.

## Acknowledgment

This work was supported by AFOSR and the Austrian Nanoinitiative project PLATON. The authors thank Dr. Stefan Birner from the Walter Schottky Institute, Technische Universitat Munchen for providing nextnano[3] software.

1) H. Schneider and H. C. Liu: *Quantum Well Infrared Photodetectors: Physics and Applications* (Springer, New York, 2007).
2) T. Ueda and S. Komiyama: Sensors **10** (2010) 8411.
3) V. Ryzhii: J. Appl. Phys. **81** (1997) 6442.
4) K. K. Choi: *The Physics of Quantum Well Infrared Photodetectors* (World Scientific, River Edge, NJ, 1997).
5) F. T. Vasko and A. Kuznetsov: *Electronic States and Optical Transitions in Semiconductor Heterostructures* (Springer, New York, 1998).
6) Y. Arslan, S. U. Eker, M. Kaldirim, and C. Besikci: Infrared Phys. Technol. **52** (2009) 399.
7) A. Kock, E. Gornik, G. Abstreiter, G. Bohm, M. Walther, and G. Weimann: Appl. Phys. Lett. **60** (1992) 2011.
8) K. L. Tsai, K. H. Chang, C. P. Lee, K. F. Huang, J. S. Tsang, and H. R. Chen: Appl. Phys. Lett. **62** (1993) 3504.
9) M. Z. Tidrow, K. K. Choi, A. J. DeAnni, W. H. Chang, and S. P. Svensson: Appl. Phys. Lett. **67** (1995) 1800.
10) H. C. Liu, J. Li, J. R. Thompson, Z. R. Wasilewski, M. Buchanan, and J. G. Simmons: IEEE Electron Device Lett. **14** (1993) 566.
11) K. K. Choi, B. F. Levine, C. G. Bethea, J. Walker, and R. J. Malik: Phys. Rev. B **39** (1989) 8029.
12) B. F. Levine, C. G. Bethea, B. O. Shen, and R. J. Malik: Appl. Phys. Lett. **57** (1990) 383.
13) E. Martinet, F. Luc, E. Rosencher, P. Bois, and S. Delaitre: Appl. Phys. Lett. **60** (1992) 895.
14) N. Vodjdani, B. Vinter, V. Berger, E. Bockenhoff, and E. Costard: Appl. Phys. Lett. **59** (1991) 555.
15) A. Majumdar, K. K. Choi, J. L. Reno, L. P. Rokhinson, and D. C. Tsu: Appl. Phys. Lett. **80** (2002) 707.
16) Z. An, T. Ueda, J.-C. Chen, S. Komiyama, and K. Hirakawa: J. Appl. Phys. **100** (2006) 044509.
17) T. Ueda, Z. An, K. Hirakawa, and S. Komiyama: J. Appl. Phys. **103** (2008) 093109.
18) T. Ueda, Z. An, K. Hirakawa, and S. Komiyama: J. Appl. Phys. **105** (2009) 064517.
19) M. Ryzhii, V. Ryzhii, R. Suris, and C. Hamaguchi: Phys. Rev. B **61** (2000) 2742.
20) M. Z. Tidrow, J. C. Chiang, S. S. Li, and K. Bacher: Appl. Phys. Lett. **70** (1997) 859.
21) H. C. Liu, M. Buchanan, and Z. R. Wasilewski: Appl. Phys. Lett. **72** (1998) 1682.
22) http://www.nextnano.de/
23) V. Mitin, L. Chien, N. Vagidov, and A. Sergeev: in *Future Trends in Microelectronics: From Nanophotonics to Sensors and Energy*, ed. S. Luryi, J. Xu, and A. Zaslavsky (Wiley–IEEE Press, Hoboken, NJ, 2010) p. 385.
24) L. Chien, A. Sergeev, V. Mitin, N. Vagidov, and S. Oktyabrsky: Nanosci. Nanotechnol. Lett. **2** (2010) 129.
25) V. Mitin, A. Antipov, A. Sergeev, N. Vagidov, D. Eason, and G. Strasser: Nanoscale Res. Lett. **6** (2011) 21.
26) A. Sergeev, V. Mitin, K. Sablon, N. Vagidov, and A. Antipov: Nanoscale Res. Lett. **6** (2011) 584.
27) L. H. Chien, A. Sergeev, N. Vagidov, V. Mitin, and S. Birner: Int. J. High Speed Electron. Syst. **20** (2011) 143.
28) G. Sarusi, B. F. Levine, S. J. Pearton, K. M. S. Bandara, and R. E. Leibenguth: Appl. Phys. Lett. **64** (1994) 960.